Comparing supernova remnants around strongly magnetized and canonical pulsars

Martin, J.; Rea, N.; Torres, D.F.; Papitto, A.

DOI
10.1093/mnras/stu1594
Publication date
2014
Document Version
Final published version
Published in
Monthly Notices of the Royal Astronomical Society

Citation for published version (APA):
Martin, J., Rea, N., Torres, D. F., & Papitto, A. (2014). Comparing supernova remnants around strongly magnetized and canonical pulsars. *Monthly Notices of the Royal Astronomical Society*, *444*(3), 2910-2924. https://doi.org/10.1093/mnras/stu1594

Monthly Notices
of the
ROYAL ASTRONOMICAL SOCIETY

MNRAS **444,** 2910–2924 (2014) doi:10.1093/mnras/stu1594

Comparing supernova remnants around strongly magnetized and canonical pulsars

J. Martin,[1★] N. Rea,[1,2] D. F. Torres[1,3] and A. Papitto[1]

[1] *Institute of Space Sciences (CSIC–IEEC), Faculty of Science, Campus UAB, Torre C5-parell, E-08193 Barcelona, Spain*
[2] *Anton Pannekoek Institute for Astronomy, University of Amsterdam, Postbus 94249, NL-1090 GE Amsterdam, the Netherlands*
[3] *Institució Catalana de Recerca i Estudis Avanats (ICREA), E-08010 Barcelona, Spain*

Accepted 2014 August 4. Received 2014 August 2; in original form 2014 April 9

ABSTRACT

The origin of the strong magnetic fields measured in magnetars is one of the main uncertainties in the neutron star field. On the other hand, the recent discovery of a large number of such strongly magnetized neutron stars is calling for more investigation on their formation. The first proposed model for the formation of such strong magnetic fields in magnetars was through alpha-dynamo effects on the rapidly rotating core of a massive star. Other scenarios involve highly magnetic massive progenitors that conserve their strong magnetic moment into the core after the explosion, or a common envelope phase of a massive binary system. In this work, we do a complete re-analysis of the archival X-ray emission of the supernova remnants (SNRs) surrounding magnetars, and compare our results with all other bright X-ray emitting SNRs, which are associated with compact central objects (which are proposed to have magnetar-like B-fields buried in the crust by strong accretion soon after their formation), high-B pulsars and normal pulsars. We find that emission lines in SNRs hosting highly magnetic neutron stars do not differ significantly in elements or ionization state from those observed in other SNRs, neither averaging on the whole remnants, nor studying different parts of their total spatial extent. Furthermore, we find no significant evidence that the total X-ray luminosities of SNRs hosting magnetars, are on average larger than that of typical young X-ray SNRs. Although biased by a small number of objects, we found that for a similar age, there is the same percentage of magnetars showing a detectable SNR than for the normal pulsar population.

Key words: line: identification – stars: magnetars – pulsars: general – ISM: supernova remnants – X-rays: general.

1 INTRODUCTION

Supernova (SN) explosions are among the most energetic and extreme events ever observed in the Universe. Supernovae (SNe) are mainly distinguished in two main classes: core-collapse (CC) and thermonuclear SNe. CCSNe result from the core collapse of a massive star ($>8\ \mathrm{M}_{\odot}$; see Woosley & Janka 2005, for a review), while thermonuclear SNe are due to the explosion of a white dwarf in a binary system with a giant star (single-degenerate origin), or from two low-mass white dwarfs in a binary system (double-degenerate origin; Hillebrandt & Niemeyer 2000). CCSNe might leave behind a fast rotating (several milliseconds) and strongly magnetized ($>10^{12}$ G) stellar core which is now made by degenerate matter: a so-called neutron star. At the same time, the envelope of the massive star, ejected at high speed ($\sim10^4\ \mathrm{km\,s^{-1}}$) into the interstellar medium (ISM), interacts with it, resulting in what is called a supernova remnant (SNR). In the standard picture, an SNR evolves in time following four main expansion phases: free expansion, Sedov–Taylor phase, radiative and merging phase. The time-scales and properties of each of those phases are characterized by the initial SN explosion energy, interstellar ambient density, and the age of the remnant (see Vink 2012 for a recent review).

In the recent years, a class of highly magnetized neutron stars (a.k.a. magnetars) have been discovered. Magnetars are a small group of X-ray pulsars (about 20 objects with spin periods between 2 and 12 s), the emission of which is not explained by the common scenario for pulsars. In fact, the very strong X-ray emission of these objects ($L_{\mathrm{x}} \sim 10^{35}$ erg) seemed too high and variable to be fed by the rotational energy alone (as in the radio pulsars), and no evidence for a companion star has been found in favour of any accretion process (see Mereghetti 2008 and Rea & Esposito 2011 for reviews). Assuming the typical magnetic loss equation for rotating neutron stars, their inferred magnetic fields appear to be in general of the

---

★ E-mail: martin@ieec.uab.es

Published by Oxford University Press on behalf of the Royal Astronomical Society

order of $B \sim 10^{14}$–10^{15} G (although low magnetic field magnetars have been recently discovered; Rea et al. 2010, 2012). Because of these high-B fields, the emission of magnetars is thought to be powered by the decay and the instability of their strong fields (Duncan & Thompson 1992; Thompson & Duncan 1993; Thompson, Lyutikov & Kulkarni 2002).

The exact mechanism playing a key role in the formation of such strong magnetic fields is currently debated; in particular, it is not clear which are the characteristics of a massive star turning into a 'magnetar' instead of a normal radio pulsar, after its SN explosion.

Preliminary calculations have shown that the effects of a turbulent dynamo amplification occurring in a newly born neutron star can indeed result in a magnetic field of a few 10^{17} G. This dynamo effect is expected to operate only in the first ∼10 s after the SN explosion of the massive progenitor, and if the protoneutron star is born with sufficiently small rotational periods (of the order of a few ms). The resulting amplified magnetic fields are expected to have a strong multipolar structure, and toroidal component (Duncan & Thompson 1992, 1996; Thompson & Duncan 1993). However, this scenario is encountering more and more difficulties: (i) if magnetic torques can indeed remove angular momentum from the core via the coupling to the atmosphere in a pre-SN phase, then the core soon after the SN might not spin rapidly enough for this convective dynamo mechanism to take place (Heger, Woosley & Spruit 2005); (ii) such a fast spinning protoneutron star would require a SN explosion one order of magnitude more energetic than normal SNe, possibly a hypernova, which is not yet clear whether it can indeed form a neutron star instead of a black hole. Recent simulations have shown that gamma ray bursts (GRBs) and hyperluminous SNe can indeed be powered by recently formed millisecond magnetars (Metzger et al. 2011; Bucciantini et al. 2012), although no observational evidence of the existence of such fast spinning and strongly magnetized neutron stars have been collected thus far.

Besides the fast spinning protoneutron star, a further idea on the origin of these high magnetic fields is that they simply reflect the high magnetic field of their progenitor stars. Magnetic flux conservation (Woltjer 1964) implies that magnetars must then be the stellar remnants of stars with internal magnetic fields of $B > 1$ kG, whereas normal radio pulsars must be the end products of less magnetic massive stars.

Recent theoretical studies showed that there is a wide spread in white dwarf progenitor magnetic fields (Wickramasinghe & Ferrario 2005), which, when extrapolated to the more massive progenitors, implies a similar wide spread in neutron star progenitors (Ferrario & Wickramasinghe 2006). Hence, apparently it seems that a fossil magnetic field might be the solution of the origin of such strongly magnetized neutron stars, without the need of invoking dynamo actions on utterly fast spinning protoneutron stars.

However, this lead to the problem of the formation of such high-B progenitor stars. The most common idea is that the magnetic field in the star reflects the magnetic field of the cloud from which the star is formed. The best studied very massive stars (around $\sim 40\ \mathrm{M}_{\odot}$) with a directly measured magnetic field are θ Orion C and HD 191612, with dipolar magnetic field of 1.1 and 1.5 kG, respectively (Donati et al. 2002, 2006). Very interestingly, the magnetic fluxes of both these stars (1.1×10^{27} G cm^2 for θ Orion C and 7.5×10^{27} G cm^2 for HD 191612) are comparable to the flux of the highest field magnetar SGR 1806−20 (5.7×10^{27} G cm^2; Woods & Thompson 2006). Other high magnetic field stars are reported in Oskinova et al. (2011).

Recent observations of the environment of some magnetars revealed strong evidence that these objects are formed from the explosion of very massive progenitors ($M > 30\ \mathrm{M}_{\odot}$). In particular: (i) a shell of H I has been detected around 1E 1048.1−5937, and interpreted as ISM displaced by the wind of a progenitor of 30–40 $\mathrm{M}_{\odot}$ (Gaensler et al. 2005); (ii) SGR 1806−20 and SGR 1900+14 have been claimed to be hosted by very young and massive star clusters, providing a limit on their progenitor mass of $>50\ \mathrm{M}_{\odot}$ (Fuchs et al. 1999; Figer et al. 2005; Davies et al. 2009) and $>20\ \mathrm{M}_{\odot}$ (Vrba et al. 2000), respectively. Finally, CXOU 010043−7211 is a member of the massive cluster Westerlund 1 (Muno et al. 2006; Ritchie et al. 2010), with a progenitor with mass estimated to be $>40\ \mathrm{M}_{\odot}$ (see also Clark et al. 2014).

Vink & Kuiper (2006) have started the idea of studying the energetics of SNRs surrounding magnetar with the aim of disentangling a possible energetic difference between those remnants and others surrounding normal pulsars. Their work did not find any clear evidence, i.e. of an additional energy released in the remnant possibly due to an excess of rotational energy at birth.

Following this study, we decided to extend their work reanalysing all available *XMM–Newton* or *Chandra* data of all confirmed and bright SNRs associated with a magnetar or with a high-B pulsar showing magnetar-like activity, and comparing in a coherent and comprehensive way all the extracted properties of these SNRs with other remnants: in particular, line ionization and X-ray luminosity. In Section 2, we report on the data analysis and reduction of our observational sample, in Section 3 the results of our analysis, and we discuss our findings in Section 4.

2 DATA ANALYSIS AND REDUCTION

In this work, our approach has tried to be as conservative and model independent as possible. In particular, our target sample has been chosen such so as to include all confirmed associations (see the McGill catalogue[1] for all proposed associations), and among those, we chose only SNRs bright enough, and with sufficiently good spectra, to perform a detailed analysis and classification of their spectral lines. We analyse the X-ray spectral lines of four SNRs hosting a neutron star that showed magnetar-like activity in its centre: Kes 73, CTB 109, N 49 and Kes 75 (see Fig. 1). We use for all targets the best available archival data: from the *XMM–Newton* telescope in the case of Kes 73, CTB 109 and N 49, and *Chandra* for Kes 75. The observations used are summarized in Table 1. To compare coherently all the spectral lines and fluxes we observed for these remnants, we have chosen to use an empirical spectral fitting for all SNRs. We have modelled all spectra using one or two Bremsstrahlung models for the spectral continuum, plus Gaussian functions for each detected spectral line. We added spectral lines one by one until the addition of a further line did not significantly improve the fit (by using the *F*-test). This approach is totally empirical, with respect to using more detailed ionized plasma models, but ensures a coherent comparison between different remnants. In Table 2, we report also the results of our spectra modelled with ionized plasma models, for a comparison with the literature.

---

[1] http://www.physics.mcgill.ca/pulsar/magnetar/main.html

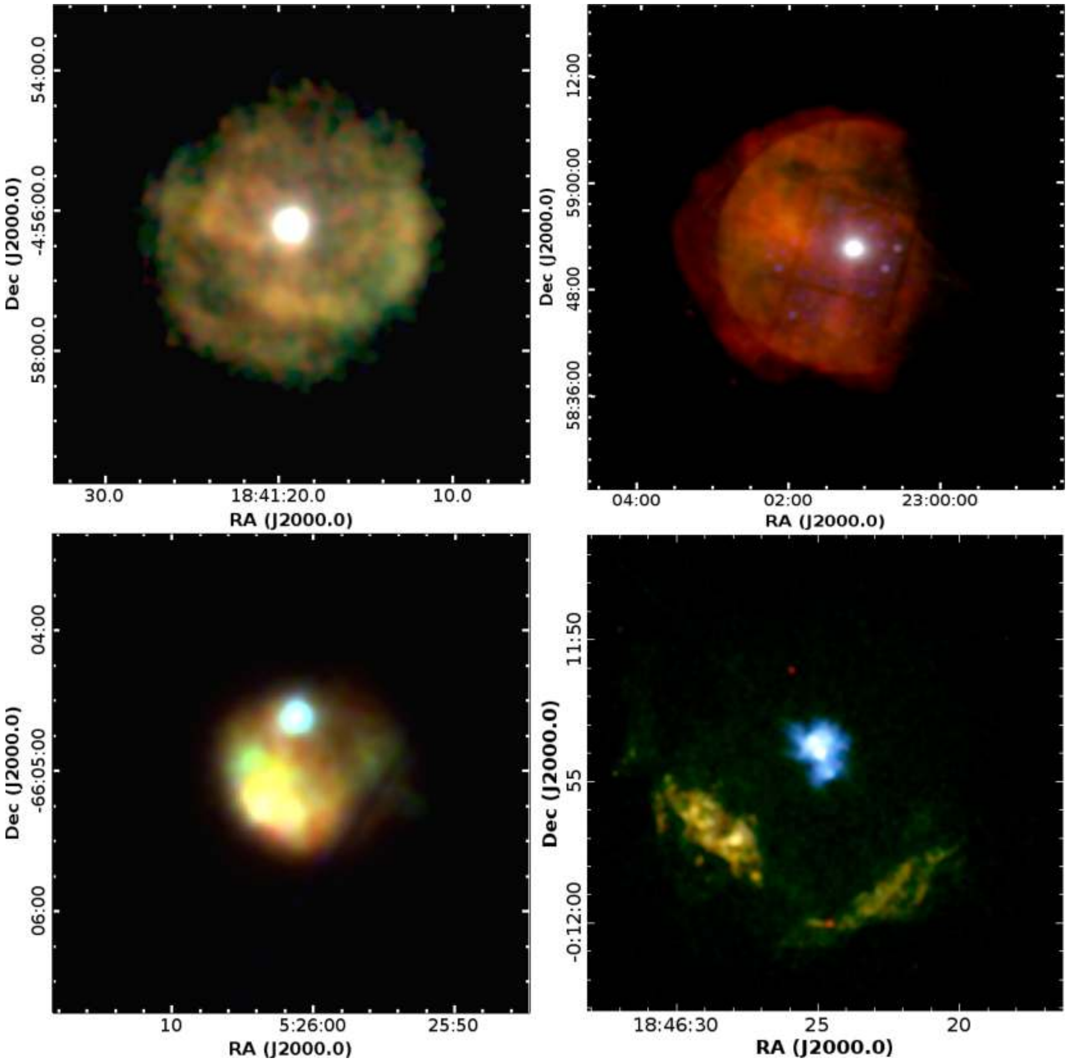

Figure 1. Combined colour images of Kes 73 (top left), CTB 109 (top right), N 49 (bottom left) and Kes 75 (bottom right).

Table 1. Observations used in this paper.

SNR	Instrument	ObsID	Date	Detector	Exp. (s)
Kes 73	*XMM*	0013340101	2002-10-05	PN	6017
				MOS1	5773
				MOS2	5771
		0013340201	2002-10-07	PN	6613
				MOS1	6372
				MOS2	6372
CTB 109	*XMM*	0057540101	2002-01-22	PN	12 237
				MOS1	19 027
				MOS2	19 026
		0057540201	2002-07-09	PN	14 298
				MOS1	17 679
				MOS2	17 679
		0057540301	2002-07-09	PN	14 011
				MOS1	17 379
				MOS2	17 379
N 49	*XMM*	0505310101	2007-11-10	PN	72 172
Kes 75	*Chandra*	748	2000-10-15	ACIS-S	37 280
		6686	2006-06-07	ACIS-S	54 070
		7337	2006-06-05	ACIS-S	17 360
		7338	2006-06-09	ACIS-S	39 250
		7339	2006-06-12	ACIS-S	44 110

2.1 *XMM–Newton* data

We use images in full-frame mode obtained from the European Photon Imaging Camera (EPIC) PN (Strüder et al. 2001) and MOS (Turner et al. 2001). The spectra of these images are fitted simultaneously in order to obtain the spectrum with the maximum possible number of counts. We used the specific software for *XMM–Newton* data, Science Analysis System (SAS) v13.5.0 with the latest calibration files. To clean images of solar flares, we used the SAS tool *tabtigen* to choose the good time intervals and extract them and the spectra with *evselect*. Source and background spectra were extracted from each single image with pattern $\leq$4 for PN images and pattern $\leq$12 for MOS. The spectra and the backgrounds corresponding to the same regions and the same detector were merged using the FTOOLS routine *mathpha* and we compute the mean of the response matrices (RMF) and the ancillary files (ARF) weighted by the exposure time using the tools *addrmf* and *addarf* (this means that we keep PN, MOS1 and MOS2 data separately and we merge the spectra when they come from the same detector). Finally, we binned the spectra demanding a minimum of 25 counts per bin to allow the use of χ^2-statistics.

We analyse the spectrum of each nebula considering its entire extension. For Kes 73, the nebula is completely covered in the

Table 2. Fits for Kes 73, CTB 109, N 49 and Kes 75 using a `vnei` plasma model. A second thermal Bremsstrahlung component is included in some cases.† The absorption column density of N 49 is fitted using the LMC abundances: He = 0.89, C = 0.30, N = 0.12, O = 0.26, Ne = 0.33, Na = 0.30, Mg = 0.32, Al = 0.30, Si = 0.30, S = 0.31, Cl = 0.31, Ar = 0.54, Ca = 0.34, Cr = 0.61, Fe = 0.36, Co = 0.30 and Ni = 0.62. We have added also the galactic absorption $N_{\mathrm{H}} = 6 \times 10^{20}$ cm^{-2}.

		`vnei`		
Parameter	Kes 73	CTB 109	N 49†	Kes 75
N_{H} (cm^{-2})	$2.51^{-0.08}_{+0.06}$	$0.695^{-0.018}_{+0.005}$	$1.03^{-0.02}_{+0.02}$	$3.71^{-0.06}_{+0.07}$
kT_{brems} (keV)	$0.41^{-0.03}_{+0.05}$	–	$0.99^{-0.01}_{+0.02}$	$0.31^{-0.04}_{+0.05}$
N_{brems} (Norm. counts s^{-1})	$0.5^{-0.2}_{+0.2}$	–	$(5.4^{-0.3}_{+0.3}) \times 10^{-3}$	$0.4^{-0.2}_{+0.5}$
kT (keV)	$1.51^{-0.08}_{+0.15}$	$0.297^{-0.004}_{+0.007}$	$0.1650^{-0.0003}_{+0.0011}$	$2.0^{-0.1}_{+0.2}$
O	1 (fixed)	$0.16^{-0.02}_{+0.01}$	$0.137^{-0.003}_{+0.002}$	1 (fixed)
Ne	1 (fixed)	$0.27^{-0.01}_{+0.01}$	$0.175^{-0.004}_{+0.004}$	1 (fixed)
Mg	$1.30^{-0.11}_{+0.09}$	$0.23^{-0.02}_{+0.01}$	$0.36^{-0.01}_{+0.01}$	$0.51^{-0.08}_{+0.09}$
Si	$1.6^{-0.1}_{0.2}$	$0.49^{-0.05}_{+0.03}$	1 (fixed)	$0.56^{-0.04}_{+0.05}$
S	$2.1^{-0.2}_{+0.4}$	1 (fixed)	1 (fixed)	$0.9^{-0.1}_{+0.2}$
Ar	$3.1^{-0.6}_{+0.9}$	1 (fixed)	1 (fixed)	$1.2^{-0.6}_{+0.8}$
Ca	6^{-2}_{+4}	1 (fixed)	1 (fixed)	1 (fixed)
Fe	1 (fixed)	$0.226^{-0.024}_{+0.008}$	1 (fixed)	1 (fixed)
E_1 (keV)	–	–	$0.729^{-0.002}_{+0.005}$	–
σ_1 (keV)	–	–	<0.07	–
N_1 (Norm. counts s^{-1})	–	–	$(5.4^{-0.3}_{+0.3}) \times 10^{-3}$	–
E_2 (keV)	–	–	$1.018^{-0.001}_{+0.001}$	–
σ_2 (keV)	–	-	<0.07	–
N_2 (Norm. counts s^{-1})	–	–	$(1.20^{-0.04}_{+0.04}) \times 10^{-3}$	–
E_3 (keV)	–	–	$1.467^{-0.008}_{+0.004}$	–
σ_3 (keV)	–	–	<0.08	–
N_3 (Norm. counts s^{-1})	–	–	$(4.9^{-0.6}_{+0.6}) \times 10^{-5}$	–
E_4 (keV)	–	–	$1.846^{-0.003}_{+0.003}$	–
σ_4 (keV)	–	–	<0.09	–
N_4 (Norm. counts s^{-1})	–	–	$(1.56^{-0.07}_{+0.07}) \times 10^{-4}$	–
E_5 (keV)	–	–	$1.998^{-0.003}_{+0.028}$	–
σ_5 (keV)	–	–	<0.09	–
N_5 (Norm. counts s^{-1})	–	–	$(5.3^{-0.5}_{+0.5}) \times 10^{-5}$	–
E_6 (keV)	–	–	$2.445^{-0.005}_{+0.005}$	–
σ_6 (keV)	–	–	<0.1	–
N_6 (Norm. counts s^{-1})	–	–	$(6.4^{-0.4}_{+0.3}) \times 10^{-5}$	–
E_7 (keV)	–	–	$3.12^{-0.02}_{+0.02}$	–
σ_7 (keV)	–	–	<0.1	–
N_7 (Norm. counts s^{-1})	–	–	$(7^{-1}_{+1}) \times 10^{-6}$	–
τ (s cm^{-3})	$(5.1^{-0.8}_{+0.6}) \times 10^{10}$	$(6.7^{-1.0}_{+0.8}) \times 10^{11}$	$(1.3^{-0.2}_{+0.1}) \times 10^{12}$	$(2.4^{-0.3}_{+0.3}) \times 10^{10}$
N (Norm. counts s^{-1})	$(3.9^{-0.9}_{+0.6}) \times 10^{-2}$	$0.35^{-0.04}_{+0.02}$	$1.69^{-0.02}_{+0.03}$	$0.021^{-0.003}_{+0.003}$
χ^2_r	1.56 (997)	2.60 (491)	1.87 (569)	1.19 (236)

EPIC PN, MOS 1 and MOS 2 detectors and we consider all of them in the analysis. In the case of CTB 109, the SNR is too large to be included entirely in a single pointing. The images with the *XMM–Newton* data ID 0057540101, 0057540201 and 0057540301 correspond to south, north and east pointings of the remnant. We computed the spectra of each pointing, also considered the EPIC PN, MOS 1 and MOS 2 cameras. For N 49, the exposure time of the MOS detectors is very low in comparison with PN. For this reason, we did not use the MOS data to avoid statistical noise in the data.

2.2 *Chandra* data

In the case of Kes 75, the best available observations were performed with *Chandra* using the Advanced CCD Imaging Spectrometer (ACIS). The ID numbers of the data used are in Table 1. We used the standard reduction software for *Chandra*, the *Chandra* Interactive Analysis of Observations (CIAO) v4.5. The spectra and the backgrounds were extracted using the routine *specextract* and the RMFs and ARFs using *mkacisrmf* and *mkwarf*, respectively. Finally, we combine the spectra demanding a minimum of 25 counts per energy bin using *combine_spectra*.

3 SPECTRAL ANALYSIS AND RESULTS

We report the fitted spectra in Fig. 3, while reporting the best-fitting models and relative parameters in Table 3. For the spectral analysis, we used the program XSPEC (Arnaud 1996) v12.8.1 from the package HEASOFT v6.15. As anticipated above, we have used for all SNRs a spectral model comprised of photoelectric absorption (`phabs`), one or two Bremsstrahlung models (`brems`), plus a series of Gaussian functions to model the emission lines. Even if more physical ionized plasma models such a `vnei`, `vshock` or `vpshock` could be used to fit those SNRs, e.g. Kumar et al. (2014) for Kes 73, Sasaki et al. (2004, 2013) for CTB 109, Park et al. (2012) for N 49 and Temim et al. (2012) for Kes 75, we prefer to use a more empirical approach to compare coherently the emission lines and luminosities of those objects, which is the aim of our work. Below, we summarize for each studied remnant our results in the context of the general properties of the SNR.

In Fig. 2, we show the background regions we have chosen for this analysis. We have tried several different regions finding consistent results. During the spectral analysis we checked that subtracting the background spectra or fitting it separately from the remnant spectra and subtracting its best-fitting model, gave consistent results.

3.1 Kes 73

Kes 73 (also known as G27.4+0.0) is a shell-type SNR. Its dimensions are about 4.7 arcmin × 4.5 arcmin and it is located between 7.5 and 9.8 kpc (Tian & Leahy 2008b). The central source is the magnetar 1E 1841−045 discovered as a compact X-ray source with the Einstein Observatory (Kriss et al. 1985), and confirmed as a magnetar in Vasisht & Gotthelf (1997) and Gotthelf, Vasisht & Dotani (1999b). The period of the magnetar is 11.78 s and its period derivative is 4.47×10^{-11} s s^{-1}. The resulting dipolar magnetic field is 7.3×10^{14} G, the spin-down luminosity is 1.1×10^{33} erg s^{-1} and the characteristic age is 4180 yr. The age of the SNR shell is estimated around 1300 yr (Vink & Kuiper 2006), which is consistent with the age between 750 and 2100 yr estimated by Kumar et al. (2014). Kes 73 has been also observed by *ROSAT* (Helfand et al. 1994), *ASCA* (Gotthelf & Vasisht 1997), *Chandra* (Lopez et al. 2011) and *Suzaku* (Sezer et al. 2010).

Kes 73 shows a quite spherical structure with 1E 1841−045 in the centre of the remnant (see Fig. 1). In the western part of the nebula (right-hand side of the images), we distinguish a shock ring which encloses the central source from west to east of the image passing below the central source. Most of the flux is emitted between 1 and 3 keV. Finally, we analysed the total spectrum of the nebula excluding a circle of 40 arcsec around the central source to exclude possible contamination from the central object. The background spectrum has been extracted from a surrounding annular region shown in Fig. 2, avoiding gaps between the CCDs to ensure good convergence of the RMF. The continuum spectrum has been fitted with two plasmas with temperatures of 0.43 and 1.34 keV. The absorption column density obtained is $N_{\rm H} = 2 \times 10^{22}$ cm^{-2}. We detected six lines. The most prominent is the Fe XXV at 6.7 keV with an equivalent width (EW) of 1.89 keV. Other lines are Mg XI at 1.35 keV (EW = 95 eV), Si XIII at 1.85 keV (EW = 0.37 keV), Si XIII at 2.19 keV (EW = 46 eV), S XV at 2.45 keV (EW = 0.38 keV) and Ar XVII at 3.13 keV (EW = 0.12 keV).

3.2 CTB 109

CTB 109 (also G109.2−1.0) was discovered in X-rays with the Einstein Observatory by Gregory & Fahlman (1980); it is 30 arcmin × 45 arcmin wide and the estimated distance is about 3 kpc (Kothes, Uyaniker & Yar 2002). The central source is the magnetar 1E 2259+586 with a spin period of 6.98 s (Fahlman & Gregory 1983) and a period derivative of 4.83×10^{-13} (Iwasawa, Koyama & Halpern 1992). The dipolar magnetic field is about 5.9×10^{13} G, the spin-down power is 5.6×10^{31} erg s^{-1} and the characteristic age is 229 kyr. Despite the large characteristic age of the pulsar, the estimated true age of the remnant is about 14 kyr (Sasaki et al. 2013). CTB 109 has been observed also in X-rays with *ASCA* (Rho, Petre & Ballet 1998), *BeppoSAX* (Parmar et al. 1998) and *ROSAT* (Hurford & Fesen 1995; Rho & Petre 1997).

The spectrum covers the entire shell and combines the three observations detailed in Table 1. The background regions used are shown in Fig. 2. We observe that the main contribution to the flux is in the energy range between 0.5 and 2 keV. Some known X-ray sources in the field of view have been excluded in our analysis.

In this case, we used two Bremsstrahlung models to fit the continuum, with temperatures of 0.07 and 0.20 keV. The measured absorption density is $N_{\rm H} = 2.83 \times 10^{22}$ cm^{-2}, and we detected 6 lines: N VII at 0.52 keV (EW = 0.74 keV) and at 0.60 keV (EW = 0.47 keV), Ne IX at 0.91 keV (EW = 0.15 keV), Ne X at 1.01 keV (EW = 68 eV), Mg XI at 1.35 keV (EW = 0.34 keV) and Si XIII at 1.86 keV (EW = 0.28 keV).

3.3 N 49

N 49 (also SNR B0525−66.1) is an SNR located in the Large Magellanic Cloud (LMC). The associated central source is SGR 0526−66 with a period of 8.047 s (Mazets et al. 1979) and a period derivative of 6.6×10^{-11} s s^{-1} (Kulkarni et al. 2003). There is some uncertainty in the association of SGR 0526−66 with N 49 (see Gaensler et al. 2001). The inferred dipolar magnetic field is 7.3×10^{14} G, the spin-down luminosity is 4.9×10^{33} erg s^{-1} and the characteristic age is ∼2 kyr. The nebula is 1.5 arcmin × 1.5 arcmin; this means that assuming a distance of 50 kpc the diameter of N 49 is ∼22 pc. Park et al. (2012) establish a Sedov age for the nebula of ∼4.8 kyr and a SN explosion energy of 1.8×10^{51} erg.

SGR 0526−66 is located in the north of the remnant. The brightest part of the nebula is in the south-east, coinciding with dense interstellar clouds (Vancura et al. 1992; Banas et al. 1997; Park et al. 2012). This part of the remnant also has contributions between 3 and 10 keV, while the contribution of the rest of the nebula is clearly negligible at this range. In Fig. 1, we show a colour image of N 49. We analyse the total spectrum of the nebula excluding a circle of 20 arcsec around the central source to avoid its contribution to the spectrum.

Table 3. Summary of the fitted models for Kes 73, CTB 109, N 49 and Kes 75.

Parameter	Kes 73	CTB 109	N 49†	Kes 75
N_{H} (10^{22} cm^{-2})	$2.00^{-0.02}_{+0.01}$	$2.83^{-0.06}_{+0.10}$	$0.698^{-0.024}_{+0.006}$	$1.79^{-0.05}_{+0.06}$
kT_1 (keV)	$0.43^{-0.05}_{+0.02}$	$0.065^{-0.002}_{+0.001}$	$0.230^{-0.003}_{+0.004}$	$2.8^{-0.1}_{+0.2}$
N_1^{brems} (Norm. counts s^{-1})	$0.36^{-0.02}_{+0.15}$	$(9^{-1}_{+14}) \times 10^{6}$	$0.512^{-0.007}_{+0.067}$	$(4.5^{-0.3}_{+0.2}) \times 10^{-3}$
kT_2 (keV)	$1.34^{-0.01}_{+0.01}$	$0.20^{-0.02}_{+0.03}$	$1.14^{-0.01}_{+0.04}$	–
N_2^{brems} (Norm. counts s^{-1})	$(2.47^{-0.06}_{+0.41}) \times 10^{-2}$	18^{-4}_{+9}	$(3.5^{-0.15}_{+0.08}) \times 10^{-3}$	–
N VII (3,4 → 1)				
E (keV)	–	$0.515^{-0.008}_{+0.016}$	–	–
σ (keV)	–	$(9.2^{-0.3}_{+0.1}) \times 10^{-2}$	–	–
N (Norm. counts s^{-1})	–	$(4^{-1}_{+4}) \times 10^{4}$	–	–
EW‡ (eV)	–	737	–	–
O VII (2,5 → 1)				
E (keV)	–	–	$0.568^{-0.004}_{+0.004}$	–
σ (keV)	–	–	$(6.1^{-0.3}_{+0.1}) \times 10^{-2}$	–
N (Norm. counts s^{-1})	–	–	$(4.7^{-0.3}_{+0.7}) \times 10^{-2}$	–
EW‡ (eV)	–	–	198	–
N VII (6,7 → 1)/O VII (2,5,6 → 1)				
E (keV)	–	$0.597^{-0.002}_{+0.003}$	–	–
σ (keV)	–	<0.06	–	–
N (Norm. counts s^{-1})	–	$(2.4^{-0.4}_{+1.5}) \times 10^{5}$	–	–
EW‡ (eV)	–	472	–	–
O VIII (6,7 → 1)/Fe XVIII (4,5 → 1)				
E (keV)	–	–	$0.769^{-0.001}_{+0.001}$	–
σ (keV)	–	–	$0.112^{-0.003}_{+0.002}$	–
N (Norm. counts s^{-1})	–	–	$(1.78^{-0.06}_{+0.11}) \times 10^{-2}$	–
EW‡ (eV)	–	–	338	–
Ne IX (2,5 → 1)				
E (keV)	–	$0.91^{-0.01}_{+0.01}$	–	–
σ (keV)	–	<0.07	–	–
N (Norm. counts s^{-1})	–	$7.2^{-0.6}_{+0.2}$	–	–
EW‡ (eV)	–	147	–	–
Ne X (3,4 → 1)				
E (keV)	–	$1.014^{-0.003}_{+0.002}$	$1.028^{-0.001}_{+0.004}$	–
σ (keV)	–	<0.07	<0.07	–
N (Norm. counts s^{-1})	–	$0.37^{-0.04}_{+0.03}$	$(5.9^{-0.3}_{+0.3}) \times 10^{-4}$	–
EW‡ (eV)	–	68	33	–
Mg XI (2 → 1)				
E (keV)	$1.346^{-0.002}_{+0.001}$	$1.347^{-0.004}_{+0.003}$	$1.332^{-0.002}_{+0.006}$	$1.33^{-0.02}_{+0.02}$
σ (keV)	<0.08	<0.08	<0.08	<0.08
N (Norm. counts s^{-1})	$(2.6^{-0.1}_{+0.1}) \times 10^{-3}$	$(2.0^{-0.1}_{+0.3}) \times 10^{-3}$	$(2.03^{-0.08}_{+0.08}) \times 10^{-4}$	$(1.8^{-0.3}_{+0.3}) \times 10^{-4}$
EW‡ (eV)	95	337	62	84
Mg XII (3,4 → 1)				
E (keV)	–	–	$1.459^{-0.005}_{+0.006}$	–
σ (keV)	–	–	<0.08	–
N (Norm. counts s^{-1})	–	–	$(3.9^{-0.5}_{+0.6}) \times 10^{-5}$	–
EW‡ (eV)	–	–	20	–
Si XIII (2,5,6,7 → 1)				
E (keV)	$1.8521^{-0.0001}_{+0.0001}$	$1.856^{-0.001}_{+0.006}$	$1.848^{-0.003}_{+0.002}$	$1.851^{-0.003}_{+0.012}$

Table 3 – *continued*

Parameter	Kes 73	CTB 109	N 49†	Kes 75
σ (keV)	<0.02	<0.02	$(2.3^{-0.6}_{+0.6}) \times 10^{-2}$	<0.02
N (Norm. counts s^{-1})	$(2.76^{-0.06}_{+0.06}) \times 10^{-3}$	$(7.0^{-0.2}_{+0.3}) \times 10^{-4}$	$(1.68^{-0.04}_{+0.06}) \times 10^{-4}$	$(2.6^{-0.1}_{+0.2}) \times 10^{-4}$
EW‡ (eV)	368	278	299	232
Si XIV (3,4 → 1)				
E (keV)	–	–	$1.998^{-0.002}_{+0.007}$	–
σ (keV)	–	–	<0.09	–
N (Norm. counts s^{-1})	–	–	$(5.2^{-0.4}_{+0.3}) \times 10^{-5}$	–
EW‡ (eV)	–	–	132	–
Si XIII (13 → 1)				
E (keV)	$2.201^{-0.010}_{+0.009}$	–	–	$2.21^{-0.02}_{+0.04}$
σ (keV)	<0.09	–	–	<0.09
N (Norm. counts s^{-1})	$(1.6^{-0.2}_{+0.2}) \times 10^{-4}$	–	–	$(3.4^{-0.9}_{+1.1}) \times 10^{-5}$
EW‡ (eV)	46	–	–	45
S XV (2,5,6,7 → 1)				
E (keV)	$2.452^{-0.002}_{+0.002}$	–	$2.444^{-0.005}_{+0.005}$	$2.437^{-0.005}_{+0.007}$
σ (keV)	<0.09	–	<0.09	<0.09
N (Norm. counts s^{-1})	$(8.0^{-0.3}_{+0.2}) \times 10^{-4}$	–	$(6.8^{-0.4}_{+0.4}) \times 10^{-5}$	$(1.09^{-0.12}_{+0.08}) \times 10^{-4}$
EW‡ (eV)	375	–	299	178
S XV (13 → 1)				
E (keV)	–	–	–	–
σ (keV)	–	–	–	–
N (Norm. counts s^{-1})	–	–	–	–
EW‡ (eV)	–	–	–	–
Ar XVII (2,5,6,7 → 1)				
E (keV)	$3.13^{-0.01}_{+0.01}$	–	$3.12^{-0.02}_{+0.02}$	–
σ (keV)	<0.1	–	<0.1	–
N (Norm. counts s^{-1})	$(9^{-1}_{+1}) \times 10^{-5}$	–	$(7^{-1}_{+1}) \times 10^{-6}$	–
EW‡ (eV)	120	–	110	–
Fe XXV (7 → 1)				
E (keV)	$6.7^{-0.2}_{+0.2}$	–	–	–
σ (keV)	$0.5^{-0.1}_{+0.2}$	–	–	–
N (Norm. counts s^{-1})	$(2.9^{-0.6}_{+0.6}) \times 10^{-5}$	–	–	–
EW‡ (eV)	1890	–	–	–
χ^2_r	1.57 (985)	2.05 (477)	1.84 (578)	1.12 (258)

†The absorption column density of N 49 is fitted using the LMC abundances: He = 0.89, C = 0.30, N = 0.12, O = 0.26, Ne = 0.33, Na = 0.30, Mg = 0.32, Al = 0.30, Si = 0.30, S = 0.31, Cl = 0.31, Ar = 0.54, Ca = 0.34, Cr = 0.61, Fe = 0.36, Co = 0.30 and Ni = 0.62. We have added also the galactic absorption $N_H = 6 \times 10^{20}$ cm^{-2}.
‡ Equivalent width.

The absorption of N 49 has two components: one is related with the Galactic absorption and the other is the absorption produced by LMC. The Milky Way photoelectric absorption towards N 49 is fixed as $N_H = 6 \times 10^{20}$ cm^{-2} (Dickey & Lockman 1990; Park et al. 2012). We include a second absorption component to take into account the absorption column density for LMC, where we use the abundances given by Russell & Dopita (1992), Hughes, Hayashi & Koyama (1998) and Park et al. (2012). We obtain an absorption column density of $N_H = 0.7 \times 10^{22}$ cm^{-2} for the LMC contribution. The continuum is represented by two Bremsstrahlung models with temperatures of 0.23 and 1.14 keV. In this case, we have detected nine lines: O VII at 0.57 keV (EW = 0.20 keV), O VIII/Fe XVIII at 0.77 keV (EW = 0.34 keV), Ne X at 1.03 keV (EW = 33 eV), Mg XI at 1.33 keV (EW = 62 eV), Mg XII at 1.46 keV (EW = 20 eV), Si XIII at 1.85 keV (EW = 0.30 keV), Si XIV at 2.00 keV (EW = 0.13 keV), S XV at 2.44 keV (EW = 0.30 keV) and Ar XVII at 3.12 keV (EW = 0.11 keV).

3.4 Kes 75

Kes 75 (G29.7−0.3) is a composite SNR. The X-ray emission of the partial shell is extended in two clouds in the south-west and south-east part of the image (see Fig. 1). It was observed first in X-rays by *Einstein* (Becker, Helfand &

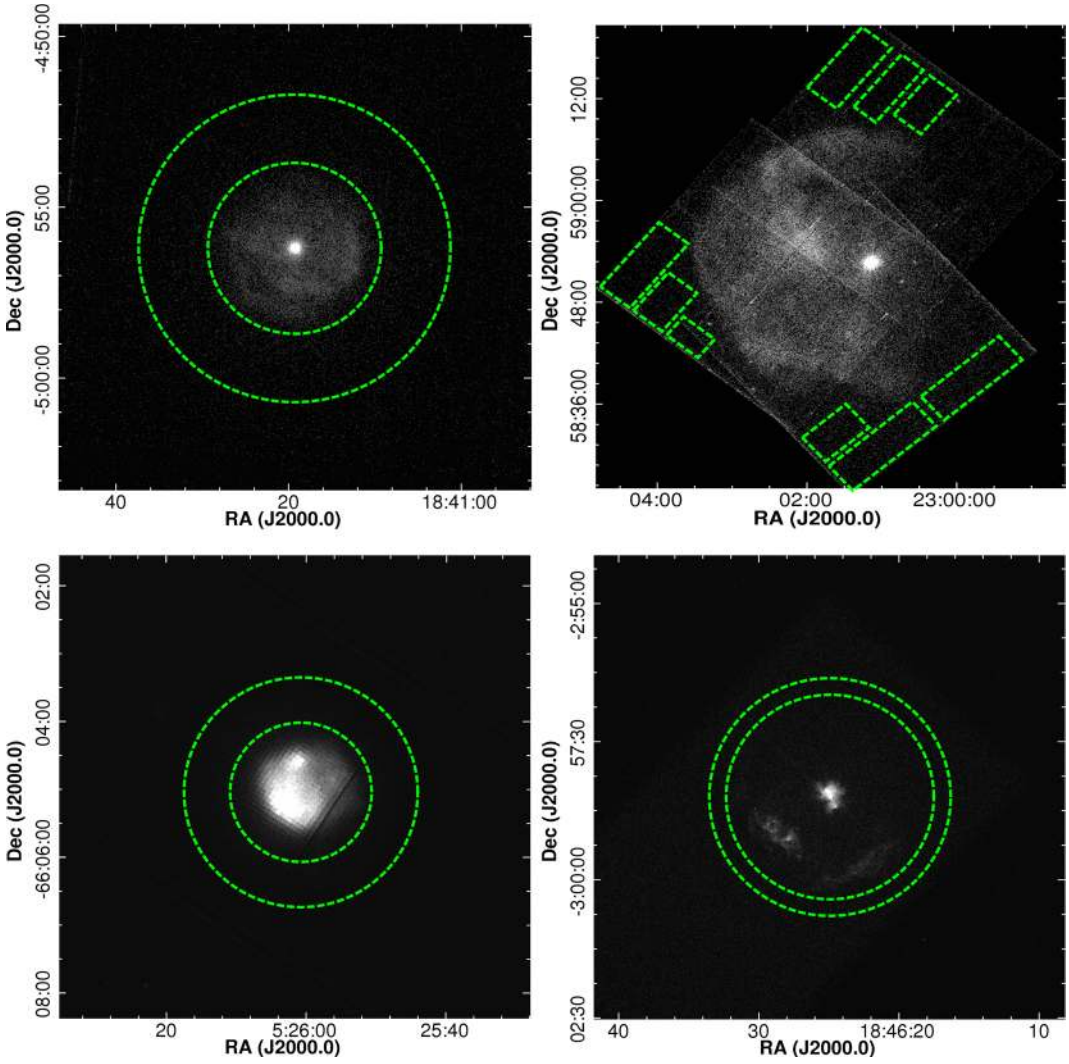

Figure 2. Map of the backgrounds used in the spectrum analysis. The order of the images is the same as in Fig. 1.

Szymkowiak 1983) showing an incomplete shell of 3 arcmin in extent. In the centre of the nebula, there is a bright pulsar wind nebula (PWN), which was spatially resolved by the *Chandra* observation (Helfand, Collins & Gotthelf 2003; Ng et al. 2008), and PSR J1846−0258 powers it. This pulsar was discovered using the *RXTE* telescope and localized within an arcminute of the remnant using *ASCA* (Gotthelf et al. 2000). The period of the pulsar is ∼326 ms and the period derivative 7.11×10^{-12} s s^{-1} (e.g. Livingstone et al. 2011). This leads to a spin-down energy loss of 8.1×10^{36} erg s^{-1}, a magnetic field of 4.9×10^{13} G and a characteristic age of 728 yr. Livingstone et al. (2006) estimated a braking index of 2.65 ± 0.01. Despite its early classification as a typical rotational powered pulsar, PSR J1846−0258 showed magnetar-like activity via short bursts and the outburst of its persistent emission (Gavriil et al. 2008; Kumar & Safi-Harb 2008) enabling its classification as (at least sporadically) a magnetically powered pulsar. There is a big uncertainty in the distance of this SNR in the literature (Caswell et al. 1975; Milne 1979; Becker & Helfand 1984; McBride, Dean & Bazzano 2008). Most recent estimates give a distance between ∼5.1 and 7.5 kpc based on H I absorption observations (Leahy & Tian 2008), and 10.6 kpc using millimetre observations of CO lines from an adjacent molecular cloud (Su et al. 2009). In our work, we adopt this value in order to compute the X-ray luminosity and the size of the SNR.

The spectrum of Kes 75 has been fitted using only one thermal Bremsstrahlung component with a temperature of 2.8 keV and an absorption column density of 1.79×10^{22} cm^{-2}. Four clear lines are resolved using Gaussians: Mg XI line at 1.33 keV (EW = 84 eV), two Si XIII lines at 1.85 (EW = 0.23 keV) and 2.21 keV (EW = 45 eV) and S XV at 2.44 keV (EW = 0.18 keV).

4 DISCUSSION

In this work, we have re-analysed in a coherent way the X-ray emission from SNRs around magnetars, and compared their emission lines and luminosities. The aim of this study was to search for any possible trend or significant difference in SNRs associated with different types of neutron stars. This work complements and extends the work by Vink & Kuiper (2006), providing a detailed description of the spectra for Kes 73, Kes 75, N 49 and CTB 109, and compares them directly with other remnants with similar spectroscopic X-ray studies. We also looked for any possible trend or significant difference in the ionization state and X-ray luminosity of SNRs associated with different types of neutron stars.

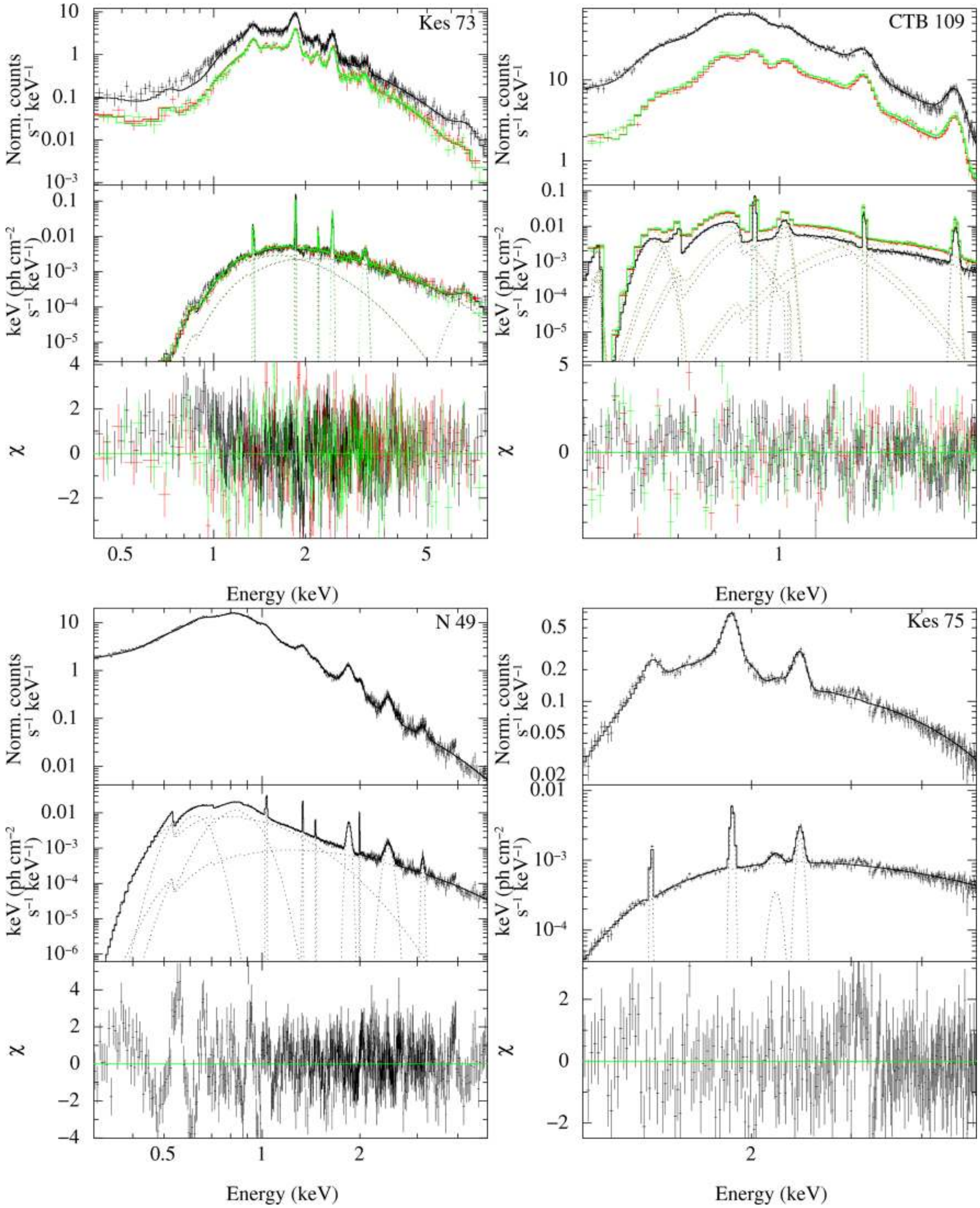

Figure 3. Spectra obtained for the Kes 73, CTB 109, N 49 and Kes 75. We used the EPIC PN (in black), MOS 1 (in red) and MOS 2 (in green) data simultaneously to fit the models.

4.1 Spectral lines comparison with other SNRs

X-ray spectra of SNRs are usually fit with plasma models (see also Table 2). In this work, we proceed to fit the spectra of Kes 73, CTB 109, N 49 and Kes 75 using a thermal Bremsstrahlung model for the continuum emission and Gaussians for the lines. Our main aim is to have an estimate of line centroid energy, to identify it properly. We have then used the simplest continuum model to reduce the free parameters of the fit.[2] One could expect that the excess of rotational energy released by the magnetar during the alpha-dynamo process could be stored in the ionization level of

---

[2] Note that in the 0.5–1 keV the detection of spectral lines are dependent on absorption model we adopted.

Table 4. Summary of line detections in X-ray for some important SNRs compared with lines detected in our analysis. The references are [1]Bleeker et al. (2001), [2]Borkowski et al. (2010), [3]Cassam-Chenaï et al. (2004), [4]Decourchelle et al. (2001), [5]Hayato et al. (2010), [6]Hwang & Gotthelf (1997), [7]Hwang, Petre & Flanagan (2008), [8]Kinugasa & Tsunemi (1987), [9]Maeda et al. (2009), [10]Miceli et al. (2009), [11]Park et al. (2007), [12]Reynolds et al. (2007), [13]Tamagawa et al. (2009), [14]Vink et al. (2004), [15]Warren & Hughes (2004), [16]Willingale et al. (2002), [17]Winkler et al. (1981a), [18]Winkler et al. (1981b), [19]Yamaguchi et al. (2008).

SNR	Galaxy	Age (yr)	Element					
			O VII (2,5,7 → 1) (0.574 KeV)	O VIII (3,4 → 1) (0.653 KeV)	O VIII (6,7 → 1) (0.774 KeV)	Ne IX (2,5 → 1) (0.915 KeV)	Ne X (3,4 → 1) (1.022 KeV)	Ne X (6,7 → 1) (1.21 KeV)
Kes 73	MW	1100–1500						
CTB 109	MW	7900–9700				X	X	
Kes 75	MW	900–4300						
N 49	LMC	5000	X		X	X	X	
G1.9+1.3 [2]	MW	110–170						
Kepler [3],[8],[12]	MW	408				X		
Tycho [4],[5],[6],[13]	MW	440				X		
SN1006 [10],[19]	MW	1006	X		X			X
Cas A [1],[9],[16]	MW	316–352	X	X	X	X	X	
MSH11-54 [11],[14]	MW	2930–3050	X	X	X	X	X	
Puppis A [7],[17],[18]	MW	3700–5500	X	X	X	X	X	X
B0509-67.5 [15]	LMC	400	X	X		X		
			Mg XI (2,5,6,7 → 1) (1.35 KeV)	Mg XII (3,4 → 1) (1.47 KeV)	Si XIII (2,5,6,7 → 1) (1.86 KeV)	Si XIV (3,4 → 1) (2.00 KeV)	Si XIII (13 → 1) (2.18 KeV)	S XV (2,5,6,7 → 1) (2.46 KeV)
Kes 73	MW	1100–1500	X		X		X	X
CTB 109	MW	7900–9700	X		X			
Kes 75	MW	900–4300	X		X		X	X
N 49	LMC	5000	X	X	X	X		X
G1.9+1.3	MW	110–170	X		X			X
Kepler	MW	408	X		X	X	X	X
Tycho	MW	440			X	X	X	X
SN1006	MW	1006	X		X			
Cas A	MW	316–352	X	X	X	X	X	X
MSH11−54	MW	2930–3050	X	X	X			X
Puppis A	MW	3700–5500	X		X		X	X
B0509−67.5	LMC	400	X		X		X	X
			S XV (13 → 1) (2.88 KeV)	Ar XVII (2,5,6,7 → 1) (3.13 KeV)	Ca XIX (2,5,6,7 → 1) (3.89 KeV)	Fe XXV *K*-shell (6.65 KeV)		
Kes 73	MW	1100–1500		X		X		
CTB 109	MW	7900–9700						
Kes 75	MW	900–4300						
N 49	LMC	5000		X				
G1.9+1.3	MW	110–170		X	X	X		
Kepler	MW	408	X	X	X	X		
Tycho	MW	440	X	X	X	X		
SN1006	MW	1006						
Cas A	MW	316–352	X	X	X	X		
MSH11−54	MW	2930–3050						
Puppis A	MW	3700–5500						
B0509−67.5	LMC	400		X	X	X		

the lines present in the spectrum. If the energy release is higher than in a normal SNR, heavy elements such as silicon (Si), sulphur (S), argon (Ar), calcium (Ca) or iron (Fe) could be systematically at a higher state of ionization. In Table 4, we collected all SNRs with detailed spectroscopic studies in the literature and we see that the typical elements detected are O VII, O VIII, Ne IX, Ne X, Mg XI, Mg XII, Si XIII, Si XIV, S XV, S XVI, Ar XVII, Ca XIX and Fe XXV. The only lines detected in all four of the spectra are the Mg XI line at 1.33 keV and Si XIII at 1.85 keV. For comparison, we also fitted the spectra of the SNRs using a `vnei` model (e. g. Borkowski, Lyerly & Reynolds 2001). The results are summarized in the Table 2. We have added a thermal Bremsstrahlung component in some cases. The temperature of the `vnei` plasma is always higher than for the thermal Bremsstrahlung, with the exception of N 49 in which the temperature for `vnei` is 0.17 keV (0.99 keV for Bremsstrahlung). The abundances obtained in both models show similar tendencies. For Kes 73 and N 49, the abundances of Si and S are quite above the solar ones. CTB 109 shows low abundances with respect to the solar ones for O, Ne, Mg, Si and Fe. Due to the complexity of the N 49 spectrum, some lines have not been reproduced well by the plasma models and we have added them using Gaussian profiles to improve the fit. In summary, our spectroscopic X-ray analysis

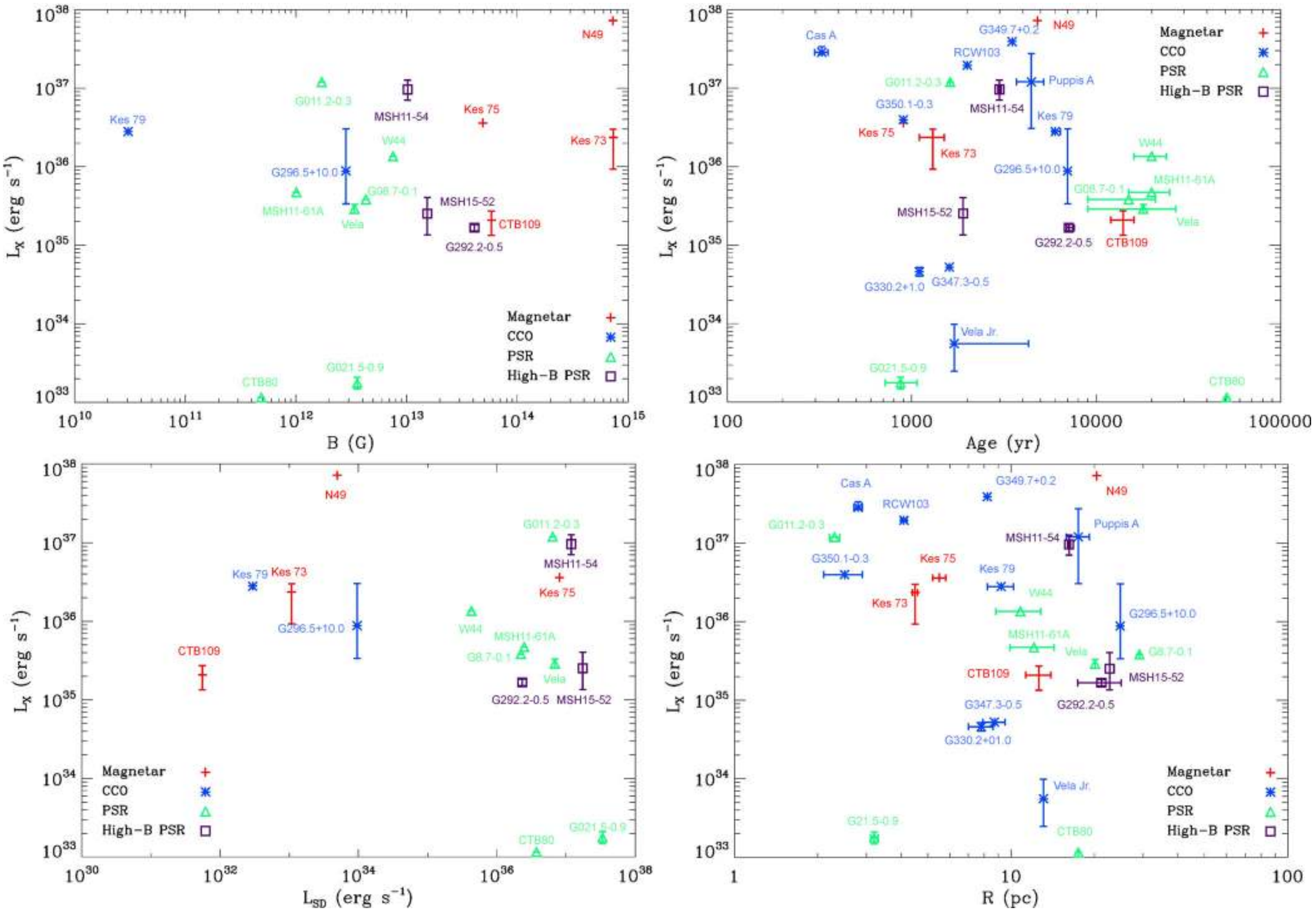

Figure 4. X-ray luminosity of all observed, and securely associated, X-ray emitting SNRs containing a magnetar, a CCO (compact central object), a high-B pulsar or a normal pulsar, plotted versus magnetic-field (top left), age (top right), spin down luminosity (bottom left) and remnant radius (bottom right).

of these sources shows compatible results with other non-magnetar SNRs already reported in literature.

4.2 Comparison with other SNRs

In Fig. 4, we have collected from the literature the X-ray luminosities from 0.5 to 10 keV of all observed SNRs brighter than $\sim 10^{33}$ erg s^{-1}, with an age lower than 100 kyr and having a confirmed association with a central source. For these remnants, we obtain the age, distance, approximate radius, magnetic field and spin-down luminosity of the central source (whenever possible) from the literature. All this information is summarized in Table 5. We have plotted the SNRs luminosities (excluding the contribution of the central neutron star luminosity) as a function of the SNR age and dimension (although note that the latter parameter is highly dependent on the environment of each remnant). For those remnants having a central neutron star with measured rotational properties, we plot the SNR luminosity as a function of the pulsar surface dipolar magnetic field at the equator ($B = 3.2 \times 10^{19}\sqrt{P\dot{P}}$ G), and the pulsar spin-down luminosity ($L_{\rm sd} = 3.9 \times 10^{46}\,\dot{P}/P^3$ erg s^{-1}; always assuming the neutron star moment of inertia $I = 10^{45}$ g cm^2), and where P is the pulsar rotation period in seconds and $\dot{P}$ its first derivative.

In order to search for any correlations in the SNRs and pulsars characteristics (see Fig. 4), we run a Spearman test. We searched for correlations between the X-ray luminosity and other features of the sources of our sample, such as dimension of the remnant, age, surface magnetic field strength and spin-down power of the associated pulsar. To this end, we employed a Spearman rank correlation test, and evaluated the significance of the value of the coefficient of correlation r obtained, by computing $t = r\sqrt{(N-2)/(1-r^2)}$, which is distributed approximately as Student's distribution with $N-2$ degrees of freedom, where N is the number of couples considered. The results we obtained are listed in Table 6; no correlation is found at a significance level larger than 99 per cent, or any significant difference in luminosity between SNRs surrounding magnetars and those around other classes of isolated neutron stars.

We have also been looking at the number of pulsars having detected SNRs as a function of age, and compared it to the magnetar case. We caution, however, that there are several systematic effects in this comparison (different detection wavebands, distance, low number of magnetars in comparison with pulsars, etc.), but we were mostly interested in looking for a general trend. In Fig. 5, we plot the result of this comparison, where we can see how on average (with all the due caveats) for a similar age, pulsars and magnetars seem to show a similar probability to have a detected SNR.

5 CONCLUSIONS

We have reported on the re-analysis of the X-ray emission of SNRs surrounding magnetars, using an empirical modelling of their spectrum with a Bremsstrahlung continuum plus several emission lines modelled by Gaussian functions. Our analysis, and the comparison

Table 5. SNRs considered in our X-ray luminosity analysis. The data without references is extracted from this work or deduced from the data obtained in the literature. The references are [1]Aharonian et al. (2007), [2]Archibald et al. (2013), [3]Aschenbach, Egger & Trümper (1995), [4]Becker et al. (2012), [5]Bietenholz & Bartel (2008), [6]Blanton & Helfand (1996), [7]Carter, Dickel & Bomans (1997), [8]Case & Bhattacharya (1998), [9]Caswell et al. (2004), [10]*Chandra* SNR catalogue*, [11]Cox et al. (1999), [12]Dodson, McCulloch & Lewis (2002), [13]Dodson et al. (2003), [14]Dubner et al. (2013), [15]Fang & Zhang (2010), [16]Ferrand & Safi-Harb (2012), [17]Fesen et al. (2006), [18]Fesen et al. (2012), [19]Finley & Oegelman (1994), [20]Frail et al. (1996), [21]Gaensler et al. (1999), [22]Gaensler & Wallace (2003), [23]Gaensler et al. (2008), [24]Giacani et al. (2000), [25]Gotthelf, Petre & Vasisht (1999a), [26]Gotthelf et al. (2000), [27]Halpern & Gotthelf (2010), [28]Hobbs et al. (2004), [29]Hughes et al. (2003), [30]Kaspi et al. (2001), [31]Katsuda, Tsunemi & Mori (2008), [32]Kellett et al. (1987), [33]Kothes et al. (2002), [34]Koyama et al. (1997), [35]Kuiper et al. (2006), [36]Kulkarni et al. (2003), [37]Kumar, Safi-Harb & Gonzalez (2012), [38]Lazendic et al. (2003), [39]Lazendic et al. (2005), [40]Livingstone et al. (2011), [41]Livingstone & Kaspi (2011), [42]Lu & Aschenbach (2000), [43]Matheson & Safi-Harb (2010), [44]Matsui, Long & Tuohy (1988), [45]Mereghetti, Tiengo & Israel (2002), [46]Mineo et al. (2001), [47]Park et al. (2009), [48]Park et al. (2012), [49]Pavlov et al. (2001), [50]Pavlov et al. (2002), [51]Pfeffermann & Aschenbach (1996), [52]Ray et al. (2011), [53]Reed et al. (1995), [54]Reynoso et al. (1995), [55]Reynoso et al. (2004), [56]Rho et al. (1994), [57]Roger et al. (1988), [58]Roy, Gupta & Lewandowski (2012), [59]Safi-Harb & Oegelman (1994), [60]Safi-Harb, Oegelman & Finley (1995), [61]Sanbonmatsu & Helfand (1992), [62]Sasaki et al. (2013), [63]Seward et al. (2003), [64]Slane et al. (2002), [65]Strom & Stappers (2000), [66]Su et al. (2009), [67]Sun et al. (2004), [68]Tam & Roberts (2003), [69]Tian & Leahy (2008a), [70]Torii et al. (1999), [71]Torii et al. (2006), [72]Vasisht & Gotthelf (1997), [73]Vink & Kuiper (2006), [74]Wang et al. (2000), [75]Weltevrede, Johnston & Espinoza (2011), [76]Winkler et al. (2009), [77]Yuan et al. (2010), [78]Zeiger et al. (2008).

Name	Central source	Distance (kpc)	Radius (pc)	Age (kyr)	$\dot{E}$ (erg s^{-1})	B_s (G)	F_X (erg cm^{-2} s^{-1})	L_X (erg s^{-1})
SNRs with magnetars								
Kes 75	J1846−0258 [26]	10.6 [66]	$5.5^{-0.3}_{+0.3}$ [10]	0.9 [6]	8.06×10^{36} [40]	4.88×10^{13} [40]	2.69×10^{-10}	3.61×10^{36}
Kes 73	1E 1841−045 [72]	$6.7^{-1.0}_{+1.8}$ [61]	$4.5^{-0.1}_{+0.1}$ [10]	$1.3^{-0.2}_{+0.2}$ [73]	1.08×10^{33} [35]	7.34×10^{14} [35]	4.39×10^{-10}	$(2.36^{-0.65}_{+1.43}) \times 10^{36}$
N 49	RX J0526−6604 [36]	50 [36]	20.4 [10]	4.8 [48]	4.92×10^{33} [36]	7.32×10^{14} [36]	2.41×10^{-10}	7.21×10^{37}
CTB 109	1E 2259+586 [2]	$3^{-0.5}_{+0.5}$ [33]	$12.6^{-1.3}_{+1.3}$ [10]	14^{-2}_{+2} [62]	5.54×10^{31} [2]	5.84×10^{13} [2]	1.94×10^{-10}	$(2.09^{-0.64}_{+0.75}) \times 10^{35}$
SNRs with CCOs								
Cas A	CXO J2323+5848 [45]	$3.4^{-0.1}_{+0.3}$ [53]	$2.8^{-0.1}_{+0.1}$ [10]	0.326^{-27}_{+27} [17]	–	–	2.06×10^{-8} [10]	$(2.85^{-0.20}_{+0.50}) \times 10^{37}$ [10]
G350.1−0.3	XMMU J1720−3726 [23]	4.5 [23]	$2.5^{-0.4}_{+0.4}$ [10]	0.9 [23]	–	–	1.64×10^{-9} [10]	3.97×10^{36} [10]
G330.2+1.0	CXOU J1601−5133 [47]	$4.9^{-0.3}_{+0.3}$ [53]	$7.8^{-0.8}_{+0.8}$ [10]	1.1 [47]	–	–	1.60×10^{-11} [71]	$(4.60^{-0.55}_{+0.57}) \times 10^{34}$ [71]
G347.3−0.5	1 WGA J1713−3949 [38]	1 [34]	$8.7^{-0.8}_{+0.8}$ [18]	1.6 [18]	–	–	4.40×10^{-10} [51]	5.26×10^{34}
Vela Jr.	CXOU J0852−4617 [49]	$0.75^{-0.55}_{+0.25}$ [35]	13.1 [10]	$1.7^{-0}_{+2.6}$ [35]	–	–	8.30×10^{-11} [1]	$(5.58^{-3.10}_{+4.34}) \times 10^{33}$
RCW 103	1E 1613−5055 [25]	3.1 [55]	$4.1^{-0.1}_{+0.1}$ [10]	2 [7]	–	–	1.70×10^{-8} [10]	1.95×10^{37}
G349.7+0.2	CXOU J1718−3726 [39]	22.4 [20]	8.2 [39]	3.5 [39]	–	–	6.50×10^{-10} [39]	3.90×10^{37}
Puppis A	RX J0822−4300 [4]	$2.2^{-0.3}_{+0.3}$ [54]	$17.5^{-1.7}_{+1.7}$ [16]	$4.45^{-0.75}_{+0.75}$ [4]	–	–	2.16×10^{-8}	$(1.20^{-0.90}_{+1.55}) \times 10^{37}$ [14]
Kes 79	J1852+0040 [63]	7.1 [8]	$9.2^{-1.0}_{+1.0}$ [10]	$6.0^{-0.2}_{+0.4}$ [67]	2.96×10^{32} [27]	3.05×10^{10} [27]	4.64×10^{-10} [67]	2.80×10^{36} [67]
G296.5+10.0	1E 1207−5209 [24]	$2.1^{-0.8}_{+1.8}$ [24]	24.8 [32]	7 [57]	9.58×10^{33} [50]	2.83×10^{12} [50]	1.67×10^{-9} [44]	$(8.81^{-5.40}_{+21.60}) \times 10^{34}$
SNRs with high-B PSRs								
MSH 15−52	J1513−5908 [21]	$5.2^{-1.4}_{+1.4}$ [15]	22.7 [46]	1.9 [15]	1.75×10^{37} [41]	1.54×10^{13} [41]	7.80×10^{-11} [46]	$(2.52^{-1.17}_{+1.54}) \times 10^{35}$
MSH 11−54	J1124−5916 [29]	$6.2^{-0.9}_{+0.9}$ [22]	$16.2^{-0.2}_{+0.2}$ [10]	$2.99^{-0.06}_{+0.06}$ [76]	1.19×10^{37} [52]	1.02×10^{13} [52]	2.09×10^{-9} [10]	$(9.61^{-2.59}_{+2.99}) \times 10^{36}$
G292.2−0.5	J1119−6127 [37]	$8.4^{-0.4}_{+0.4}$ [9]	$21.1^{-3.8}_{+3.8}$ [10]	$7.1^{-0.2}_{+0.5}$ [37]	2.34×10^{36} [75]	4.10×10^{13} [75]	1.98×10^{-11} [37]	$(1.67^{-0.15}_{+0.16}) \times 10^{35}$
SNRs with normal PSRs								
G21.5−0.9	J1833−1034 [43]	$4.7^{-0.4}_{+0.4}$ [69]	$3.2^{-0.1}_{+0.1}$ [10]	$0.87^{-1.5}_{+2.0}$ [5]	3.37×10^{37} [58]	3.58×10^{12} [58]	6.69×10^{-13}	$(1.77^{-0.31}_{+0.29}) \times 10^{33}$ [43]
G11.2−0.3	J1811−1925 [70]	5 [30]	$2.3^{-0.1}_{+0.1}$ [10]	1.616 [68]	6.42×10^{36} [70]	1.71×10^{12} [70]	3.98×10^{-9} [10]	1.19×10^{37} [10]
G8.7−0.1	J1803−2137 [19]	4 [19]	29.1 [19]	15^{-6}_{+6} [19]	2.22×10^{36} [77]	4.92×10^{12} [77]	2.00×10^{-10} [19]	3.83×10^{35}
Vela	J0835−4510 [3]	$0.287^{-0.017}_{+0.019}$ [13]	20.1 [42]	18^{-9}_{+9} [3]	6.92×10^{36} [12]	3.38×10^{12} [12]	2.94×10^{-8}	$(2.90^{-0.34}_{+0.39}) \times 10^{35}$ [42]
MSH 11−61A	J1105−6107 [64]	7 [64]	$12.1^{-2.2}_{+2.2}$ [64]	20^{-5}_{+5} [64]	2.48×10^{36} [74]	1.01×10^{12} [74]	8.06×10^{-11} [10]	4.71×10^{35} [10]
W 44	J1856+0113 [11]	2.5 [11]	$10.8^{-2.0}_{+2.0}$ [11]	20^{-4}_{+4} [11]	4.30×10^{35} [28]	7.55×10^{12} [28]	1.80×10^{-9} [56]	1.35×10^{36}
CTB 80	J1952+3252 [60]	2 [65]	1.5 [60]	51 [78]	3.74×10^{36} [28]	4.86×10^{11} [28]	2.40×10^{-12}	1.15×10^{33} [59]

*http://hea-www.cfa.harvard.edu/ChandraSNR/

of the emission of those remnants with other bright SNR surrounding normal pulsars suggest the following conclusions.

(i) We find no evidence of generally enhanced ionization states in the elements observed in magnetars' SNRs compared to remnants observed around lower magnetic pulsars.

(ii) No significant correlation is observed between the SNRs' X-ray luminosities and the pulsar magnetic fields.

(iii) We show evidence that the percentage of magnetars and pulsars hosted in a detectable SNR are very similar, at a similar age.

Our findings do not support the claim of magnetars being formed via more energetic SNe, or having a large rotational energy budget at birth that is released in the surrounding medium in the first phases of the magnetar formation. However, we note that although we do not find any hint in the SNRs to support such an idea, we cannot exclude that: (1) most of the rotational energy has been emitted via neutrinos or gravitational waves, hence with no interaction with the remnant; or (2) we are restricted to a very small sample, and with larger statistics some correlation might be observed in the future.

Table 6. Spearman correlation coefficient (r), number of couples considered (N) and probability that the two samples are not correlated (p) evaluated by comparing the X-ray luminosity of the sources of our sample with the age, radius, surface magnetic field strength and spin-down luminosity.

Parameters	r	N	p
L_X versus age	− 0.158	24	0.46
L_X versus radius	− 0.245	24	0.25
L_X versus B	0.271	16	0.31
L_X versus L_{sd}	− 0.309	16	0.25

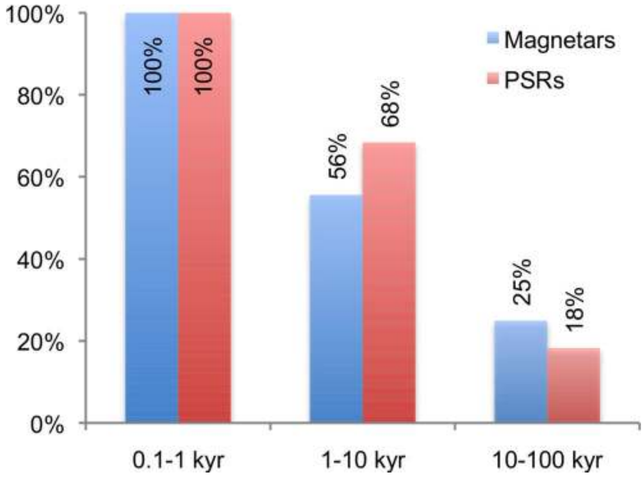

Figure 5. Percentage of pulsars and magnetars having a detected SNR as a function of the age.

ACKNOWLEDGEMENTS

This work was supported by grants AYA2012-39303, SGR2009-811, iLINK 2011-0303 and the NewCOMPSTAR MP1304 COST Action. NR is supported by a Ramón y Cajal fellowship and by an NWO Vidi Award. AP is supported by a Juan de la Cierva fellowship. We are indebted to Samar Safi-Harb and Harsha Kumar for providing the *Chandra* data on Kes 75, and for useful comments. We also thank Manami Sasaki and the referee for comments and suggestions that improved the manuscript.

REFERENCES

Aharonian F. et al., 2007, ApJ, 661, 236
Archibald R. F. et al., 2013, Nature, 497, 591
Arnaud K. A., 1996, Jacoby G., Barnes J., eds, ASP Conf. Ser. Vol. 101, Astronomical Data Analysis Software and Systems V. Astron. Soc. Pac., San Francisco, p. 17
Aschenbach B., Egger R., Trümper J., 1995, Nature, 373, 587
Banas K. R., Hughes J. P., Bronfman L., Nyman L., 1997, ApJ, 480, 607
Becker R. H., Helfand D. J., 1984, ApJ, 283, 154
Becker R. H., Helfand D. J., Szymkowiak A. E., 1983, ApJ, 268, L93
Becker W., Prinz T., Winkler P. F., Petre R., 2012, ApJ, 755, 141
Bietenholz M. F., Bartel N., 2008, MNRAS, 386, 1411
Blanton E. L., Helfand D. J., 1996, ApJ, 470, 961
Bleeker J. A., Willingale R., van der Heyden K., Dennerl K., Kaastra J. S., Aschenbach B., Vink J., 2001, A&A, 365, L225
Borkowski K. J., Lyerly W. J., Reynolds S. P., 2001, ApJ, 548, 820
Borkowski K. J., Reynolds S. P., Green D. A., Hwang U., Petre R., Krishnamurthy K., Willett R., 2010, ApJ, 724, L161
Bucciantini N., Metzger B. D., Thompson T. A., Quataert E., 2012, MNRAS, 419, 1537
Carter L. M., Dickel J. R., Bomans D. J., 1997, PASP, 109, 990
Case G. L., Bhattacharya D., 1998, ApJ, 504, 761
Cassam-Chenaï G., Decourchelle A., Ballet J., Hwang U., Hughes J. P., Petre R., 2004, A&A, 414, 545
Caswell J. L., Murray J. D., Roger R. S., Cole D. J., Cooke D. J., 1975, A&A, 45, 239
Caswell J. L., McClure-Griffiths N. M., Cheung M. C. M., 2004, MNRAS, 352, 1405
Clark J. S., Ritchie B. W., Najarro F., Langer N., Negueruela I., 2014, A&A, 565, 90
Cox D. P., Shelton R. L., Maciejewski W., Smith R. K., Plewa T., Pawl A., Różyczka M., 1999, ApJ, 524, 179
Davies B., Figer D. F., Kudritzki R.-P., Trombley C., Kouveliotou C., Wachter S., 2009, ApJ, 707, 844
Decourchelle A. et al., 2001, A&A, 365, L218
Dickey J. M., Lockman F. J., 1990, ARA&A, 28, 215
Dodson R. G., McCulloch P. M., Lewis D. R., 2002, ApJ, 564, L85
Dodson R. G., Legge D., Reynolds J. E., McCulloch P. M., 2003, ApJ, 596, 1137
Donati J. F., Babel J., Harries T. J., Howarth I. D., Petit P., Semel M., 2002, MNRAS, 333, 55
Donati J. F., Howarth I. D., Bouret J. C., Petit P., Catala C., Landstreet J., 2006, MNRAS, 365, 6
Dubner G., Loiseau N., Rodríguez-Pascual P., Smith M. J. S., Giacani E., Castelletti G., 2013, A&A, 555, A9
Duncan R. C., Thompson C., 1992, ApJ, 392, L9
Duncan R. C., Thompson C., 1996, in Rothschild R. E., Lingenfelter R. E., eds, AIP Conf. Proc. Vol. 366, High Velocity Neutron Stars and Gamma-Ray Bursts. Am. Inst. Phys., New York, p. 111
Fahlman G. G., Gregory P. C., 1983, in Danziger J., Gorenstein P., eds, Proc. IAU Symp. 101, Supernova Remnants and Their X-Ray Emission. Kluwer, Dordrecht, p. 445
Fang J., Zhang L., 2010, A&A, 515, 20
Ferrand G., Safi-Harb S., 2012, Adv. Space Res., 49, 1313
Ferrario L., Wickramasinghe D., 2006, MNRAS, 367, 1323
Fesen R. A. et al., 2006, ApJ, 645, 283
Fesen R. A., Kremer R., Patnaude D., Milisavljevic D., 2012, AJ, 143, 27
Figer D. F., Najarro F., Gaballe T. R., Blum R. D., Kudritzki R. P., 2005, ApJ, 622, L49
Finley J. P., Oegelman H., 1994, ApJ, 434, L25
Frail D. A., Goss W. M., Reynoso E. M., Giacani E. B., Green A. J., Otrupcek R., 1996, AJ, 111, 1651
Fuchs Y., Mirabel F., Chaty S., Claret A., Cesarsky C. J., Cesarsky D. A., 1999, A&A, 350, 891
Gaensler B. M., Wallace B. J., 2003, ApJ, 594, 326
Gaensler B. M., Brazier K. T. S., Manchester R. N., Johnston S., Green A. J., 1999, MNRAS, 305, 724
Gaensler B. M., Slane P. O., Gotthelf E. V., Vasisht G., 2001, ApJ, 486, L133
Gaensler B. M., McClure-Griffiths N. M., Oey M. S., Haverkorn M., Dickey J. M., Green A. J., 2005, ApJ, 620, L95
Gaensler B. M. et al., 2008, ApJ, 680, L37
Gavriil F. P., Gonzalez M. E., Gotthelf E. V., Kaspi V. M., Livingstone M. A., Woods P. M., 2008, Science, 319, 1802
Giacani E. B., Dubner G. M., Green A. J., Goss W. M., Gaensler B. M., 2000, AJ, 119, 281
Gotthelf E. V., Vasisht G., 1997, ApJ, 486, L133
Gotthelf E. V., Petre R., Vasisht G., 1999, ApJ, 514, L107
Gotthelf E. V., Vasisht G., Dotani T., 1999, ApJ, 522, L49
Gotthelf E., Vasisht G., Boylan-Kolchin M., Torii K., 2000, ApJ, 542, L37
Gregory P. C., Fahlman G. G., 1980, Nature, 287, 805
Halpern J. P., Gotthelf E. V., 2010, ApJ, 709, 436
Hayato A. et al., 2010, ApJ, 725, 894
Heger A., Woosley S. E., Spruit H. C., 2005, ApJ, 626, 350
Helfand D. J., Becker R. H., Hawkins G., White R. L., 1994, ApJ, 434, 627
Helfand D. J., Collins B. F., Gotthelf E. V., 2003, ApJ, 582, 783

Hillebrandt W., Niemeyer J. C., 2000, ARA&A, 38, 191

Hobbs G., Lyne A. G., Kramer M., Martin C. E., Jordan C., 2004, MNRAS, 353, 1311

Hughes J. P., Hayashi I., Koyama K., 1998, ApJ, 505, 732

Hughes J. P., Slane P. O., Park S., Roming P. W. A., Burrows D. N., 2003, ApJ, 591, L139

Hurford A. P., Fesen R. A., 1995, MNRAS, 277, 549

Hwang U., Gotthelf E. V., 1997, ApJ, 475, 665

Hwang U., Petre R., Flanagan K. A., 2008, ApJ, 676, 378

Iwasawa K., Koyama K., Halpern J. P., 1992, PASJ, 44, 9

Kaspi V. M., Roberts M. E., Vasisht G., Gotthelf E. V., Pivovaroff M., Kawai N., 2001, ApJ, 560, 371

Katsuda S., Tsunemi H., Mori K., 2008, ApJ, 678, L35

Kellett B. J., Branduardi-Raymont G., Culhane J. L., Mason I. M., Mason K. O., Whitehouse D. R., 1987, MNRAS, 225, 199

Kinugasa K., Tsunemi H., 1999, PASJ, 51, 239

Kothes R., Uyaniker B., Yar A., 2002, ApJ, 576, 169

Koyama K., Kinugasa K., Matsuzaki K., Nishiuchi M., Sugizaki M., Torii Ken'ichi., Yamauchi S., Aschenbach B., 1997, PASJ, 49, L7

Kriss G. A., Becker R. H., Helfand D. J., Canizares C. R., 1985, ApJ, 288, 703

Kuiper L., Hermsen W., den Hartog P. R., Collmar W., 2006, ApJ, 645, 556

Kulkarni S. R., Kaplan D. L., Marshall H. L., Frail D. A., Murakami T., Yonetoku D., 2003, ApJ, 585, 948

Kumar H. S., Safi-Harb S., 2008, ApJ, 678, 43

Kumar H. S., Safi-Harb S., Gonzalez M. E., 2012, ApJ, 754, 96

Kumar H. S., Safi-Harb S., Slane P. O., Gotthelf E. V., 2014, ApJ, 781, 41

Lazendic J. S., Slane P. O., Gaensler B. M., Plucinsky P. P., Hughes J. P., Galloway D. K., Crawford F., 2003, ApJ, 593, L27

Lazendic J. S., Slane P. O., Hughes J. P., Chen Y., Dame T. M., 2005, ApJ, 618, 733

Leahy D. A., Tian W. W., 2008, A&A, 480, L25

Livingstone M. A., Kaspi V. M., 2011, ApJ, 742, 31

Livingstone M. A., Kaspi V. M., Gotthelf E. V., Kuiper L., 2006, ApJ, 647, 1286

Livingstone M. A., Ng C.-Y., Kaspi V. M., Gavriil F. P., Gotthelf E. V., 2011, ApJ, 730, 66

Lopez L. A., Ramirez-Ruiz E., Huppenkothen D., Badenes C., Pooley D. A., 2011, ApJ, 732, 114

Lu F. J., Aschenbach B., 2000, A&A, 362, 1083

McBride V. A., Dean A. J., Bazzano F., 2008, A&A, 477, 249

Maeda Y. et al., 2009, PASJ, 61, 1217

Matheson H., Safi-Harb S., 2010, ApJ, 724, 572

Matsui Y., Long K. S., Tuohy I. R., 1988, ApJ, 329, 838

Mazets E. P., Golenetskii S. V., Il'inskii V. N., Aptekar R. L., Guryan Y. A., 1979, Nature, 282, 587

Mereghetti S., 2008, A&AR, 15, 225

Mereghetti S., Tiengo A., Israel G. L., 2002, ApJ, 569, 275

Metzger B. D., Giannios D., Thompson T. A., Bucciantini N., Quataert E., 2011, MNRAS, 413, 2031

Miceli M. et al., 2009, A&A, 501, 239

Milne D. K., 1979, Aust. J. Phys., 32, 83

Mineo T., Cusumano G., Maccarone M. C., Massaglia S., Massaro E., Trussoni E., 2001, A&A, 380, 695

Muno M. P. et al., 2006, ApJ, 636, L41

Ng C.-Y., Slane P. O., Gaensler B. M., Hughes J. P., 2008, ApJ, 686, 508

Oskinova L. M., Todt H., Ignace R., Brown J. C., Cassinelli J. P., Hamann W.-R., 2011, MNRAS, 416, 1456

Park S., Hughes J. P., Slane P. O., Burrows D. N., Gaensler B. M., Ghavamian P., 2007, ApJ, 670, L121

Park S., Kargaltsev Oleg., Pavlov G. G., Mori K., Slane P. O., Hughes J. P., Burrows D. N., Garmire G. P., 2009, ApJ, 695, 431

Park S., Hughes J. P., Slane P. O., Burrows D. N., Lee J.-J., Mori K., 2012, ApJ, 748, 117

Parmar A. N., Oostrebroek T., Favata F., Pightling S., Coe M. J., Mereghetti S., Israel G. l., 1998, A&A, 330, 175

Pavlov G. G., Sanwal D., Kiziltan B., Garmire G. P., 2001, ApJ, 559, L131

Pavlov G. G., Zavlin V. E., Sanwal D., Trümper J., 2002, ApJ, 569, L95

Pfeffermann E., Aschenbach B., 1996, in Zimmermann H. U., Trümper J. E., Yorke H., eds, Proc. Int. Conf. X-ray Astron. Astrophys.: Röntgenstrahlung from the Universe. Max-Planck-Institut für Extraterrestrische Physik, Garching, p. 267

Ray P. S. et al., 2011, ApJS, 194, 17

Rea N., Esposito P., 2011, High-Energy Emission from Pulsars and their Systems. Springer-Verlag, Berlin, p. 247

Rea N. et al., 2010, Science, 330, 944

Rea N. et al., 2012, ApJ, 754, 27

Reed J. E., Hester J. J., Fabian A. C., Winkler P. F., 1995, ApJ, 440, 706

Reynolds S. P., Borkowski K. J., Hwang U., Hughes J. P., Badenes C., Laming J. M., Blondin J. M., 2007, ApJ, 668, L135

Reynoso E. M., Dubner G. M., Goss W. M., Arnal E. M., 1995, AJ, 110, 318

Reynoso E. M., Green A. J., Johnston S., Goss W. M., Dubner G. M., Giacani E. B., 2004, PASA, 21, 82

Rho J. H., Petre R., 1997, ApJ, 484, 828

Rho J. H., Petre R., Schlegel E. M., Hester J. J., 1994, ApJ, 430, 757

Rho J. H., Petre R., Ballet J., 1998, Adv. Space Res., 22, 1039

Ritchie B. W., Clark J. S., Negueruela N., Langer N., 2010, A&A, 520, A48

Roger R. S., Milne D. K., Kesteven M. J., Wellington K. J., Haynes. R F., 1988, ApJ, 332, 940

Roy J., Gupta Y., Lewandowski W., 2012, MNRAS, 424, 2213

Russell S. C., Dopita M. A., 1992, ApJ, 384, 508

Safi-Harb S., Oegelman H., Finley J. P., 1994, BAAS, 184, 5603

Safi-Harb S., Oegelman H., Finley J. P., 1995, ApJ, 439, 722

Sanbonmatsu K. Y., Helfans D. J., 1992, AJ, 104, 2189

Sasaki M., Plucinsky P. P., Gaetz T. J., Smith R. K., Edgar R. J., Slane P. O., 2004, ApJ, 617, 322

Sasaki M., Plucinsky P. P., Gaetz T. J., Bocchino F., 2013, A&A, 552, 45

Seward F. D., Slane P. O., Smith R. K., Sun M., 2003, ApJ, 584, 414

Sezer A., Gök F., Hudaverdi M., Aktekin E., Ercan E. N., 2010, in Tsinganos K., Hatzidimitriou D., Matsakos T., eds, ASP Conf. Ser. Vol. 424, Advances in Hellenic Astronomy during the IYA09. Astron. Soc. Pac., San Francisco, p. 171

Slane P. O., Smith R. K., Hughes J. P., Petre R., 2002, ApJ, 564, 284

Strom R. G., Stappers B. W., 2000, in Kramer M., Wex N., Wielebinski N., eds, ASP Conf. Ser. Vol. 202, IAU Colloq. 177: Pulsar Astronomy - 2000 and Beyond. Astron. Soc. Pac., San Francisco, p. 509

Strüder L. et al., 2001, A&A, 365, L18

Su Y., Chen Y., Yang J., Koo B.-C., Zhou X., Jeong I.-G., Zhang C.-G., 2009, ApJ, 694, 376

Sun M., Seward F. D., Smith R. K., Slane P. O., 2004, ApJ, 605, 742

Tam C., Roberts M. S. E., 2003, ApJ, 598, L27

Tamagawa T. et al., 2009, PASJ, 61, S167

Temim T., Slane P., Arendt R. G., Dwek E., 2012, ApJ, 745, 46

Thompson C., Duncan R. C., 1993, ApJ, 408, 194

Thompson C., Lyutikov M., Kulkarni S. R., 2002, ApJ, 574, 332

Tian W. W., Leahy D. A., 2008a, MNRAS, 391, L54

Tian W. W., Leahy D. A., 2008b, ApJ, 677, 292

Torii K., Tsunemi H., Dotani T., Mitsuda K., Kawai N., Kinugasa K., Saito Y., Shibata S., 1999, ApJ, 523, L69

Torii K., Uchida H., Hasuike K., Tsunemi H., Yamaguchi Y., Shibata S., 2006, PASJ, 58, L11

Turner M. J. L. et al., 2001, A&A, 365, L27

Vancura O., Blare W. P., Long K. S., Raymond J. C., 1992, ApJ, 394, 158

Vasisht G., Gotthelf E. V., 1997, ApJ, 486, L129

Vink J., 2012, A&AR, 20, 49

Vink J., Kuiper L., 2006, MNRAS, 370, L14

Vink J., Bleeker J., Kaastra J. S., Rasmussen A., 2004, Nucl. Phys. B, 132, 62

Vrba F. J., Henden A. A., Luginbuhl C. B., Guetter H. H., 2000, ApJ, 533, L17

Wang N., Manchester R. N., Pace R. T., Bailes M., Kaspi V. M., Stappers B. W., Lyne A. G., 2000, MNRAS, 317, 843

Warren J. S., Hughes J. P., 2004, ApJ, 608, 261

Weltevrede P., Johnston S., Espinoza C. M., 2011, MNRAS, 411, 1917

Wickramasinghe D. T., Ferrario L., 2005, MNRAS, 356, 1576

Willingale R., Bleeker J. A., van der Heyden K. J., Kaastra J. S., Vink J., 2002, A&A, 381, 1039

Winkler P. F., Canizares C. R., Clark G. W., Markert T. H., Petre R., 1981a, ApJ, 245, 574

Winkler P. F., Clark G. W., Markert T. H., Kalata K., Schnopper H. W., Canizares C. R., 1981b, ApJ, 246, L27

Winkler P. F., Twelker K., Reith C. N., Long K. S., 2009, ApJ, 692, 1489

Woltjer L., 1964, ApJ, 140, 1309

Woods P. M., Thompson C., 2006, Cambridge Astrophysics Series, Vol. 39, Compact Stellar X-ray Sources. Cambridge Univ. Press, Cambridge, p. 547

Woosley S., Janka T., 2005, Nature, 1, 147

Yamaguchi H. et al., 2008, PASJ, 60, S141

Yuan J. P., Wang N., Manchester R. N., Liu Z. Y., 2010, MNRAS, 404, 289

Zeiger B. R., Brisken W. F., Chatterjee S., Goss W. M., 2008, ApJ, 674, 271

This paper has been typeset from a TEX/LATEX file prepared by the author.